INTERNATIONAL JOURNAL FOR NUMERICAL METHODS IN FLUIDS, VOL. 19, 815–825 (1994)

SIMULATION OF SUPERSONIC FLOWS WITH DETACHED SHOCKS USING A PROPERTY CONVECTION METHOD

J. F. MILTHORPE

University College, University of New South Wales, Campbell, NSW 2600, Australia

SUMMARY

An algorithm based on the convection of fundamental flow quantities, i.e. mass, momentum and energy, has been described by the author previously.[1] Computer codes to implement the algorithm have been developed for two-dimensional and axisymmetric flows. This algorithm has been further developed to improve the accuracy and stability of the calculations. In this paper the algorithm is used to calculate the flows about two-dimensional and axisymmetric bluff bodies. Bodies of practical interest in supersonic and hypersonic flows are often sufficiently bluff for a detached shock to develop, and correct prediction of the shock stand-off distance and the position of the sonic line is a useful test of numerical methods.

The programme is used to calculate flows with a detached shock around three standard shapes: a sphere, a body of revolution with a flat nose and a plate with a flat nose. The Mach number range for the flows described is from 1·177 to 6·0. Comparisons are given with standard experimental results for the steady state stand-off.

KEY WORDS Supersonic Navier–Stokes Bluff bodies Detached shocks

INTRODUCTION

Most practical problems in supersonic flow involve bluff bodies with detached shocks, and prediction of the shock shape and stand-off distance is still unreliable. When a detached shock develops, a significant region of the flow field is subsonic: around the stagnation point the velocity is naturally very small. Some common computational techniques, e.g. parabolized Navier–Stokes (PNS), become invalid in such regions. The algorithm used in this paper has been described previously and shown to give good predictions for supersonic flows with attached shocks.[1–4] Prediction of the shock shape and stand-off distance for flows around bluff bodies offers a strong test for numerical methods, since experimental data are available for flows around a wide variety of bluff shapes. Commonly tested shapes include a sphere, a cylinder with a blunt end lengthwise in the flow and a blunt flat plate. This paper reports the testing of the algorithm in a variety of flows with detached shocks at low supersonic Mach numbers.

CONSERVATION ALGORITHM

The algorithm used to calculate the flow values is based on conservation of mass, momentum and energy as the simulation proceeds over discrete time steps. The flow domain is divided into rectangular cells. At any given time, each cell contains a certain block of material which possesses a certain momentum and energy. In the course of the next time step this block, with its associated

CCC 0271–2091/94/210815–11

Received November 1993
Revised April 1994

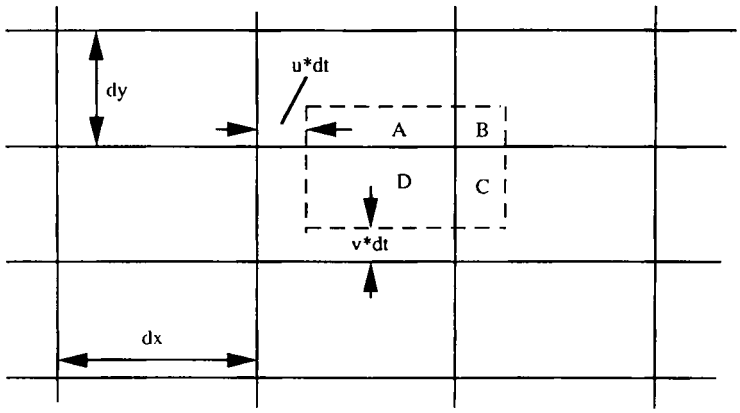

Figure 1. Convection of material block with velocities u and v during one timestep dt. See text for description of convection algorithm.

mass, momentum and energy, is convected a small distance. It may also gain or lose mass, momentum or energy by diffusion and by the action of pressure gradients. The algorithm evaluates the changes in these quantities for the material block. The process is illustrated in Figure 1 for convection with positive velocities u and v. The letters A, B, C, and D represent the proportion of the material block located in a particular cell at the end of a time step dt. These proportions of the quantities in the material block are allocated to their respective cells. When the process has been performed for all cells, the new distribution of mass, momentum and energy is available. From this distribution updated values of density, velocity, pressure and temperature can be derived. Partial upwinding is used in the evaluation of the momentum and energy changes produced by the pressure gradients, to prevent instabilities.

The flow quantities are transported by three processes modelled by the algorithm. These are diffusive transport of mass, momentum and energy, mechanical transport of momentum and energy due to pressure differences between the cells, and convective transport of mass, momentum and energy due to the velocity of the fluid relative to the mesh of cells.

Calculation of the flow quantities at the next time step is done in the following sequence. The mass, momentum and energy in a cell are modified by the action of diffusion. The momentum and energy in the cell are then modified by the action of the pressure gradients. The pressure difference between adjacent cells moves momentum between the cells. It has been necessary to use local upwinding in the evaluation of the momentum transport due to pressure gradients. The upwinding velocity at a cell is taken as the average velocity over a group of 24 surrounding cells. The x-momentum transported into the cell i, j is calculated as

$$\delta(\rho u) = \delta t \, dy \tfrac{1}{2}[(1 + F)p_{i-1,j} + 2Fp_{i,j} - (1 - F)p_{i+1,j}]. \tag{1}$$

Here F is the upwinding factor such that $F = 1$ gives complete upwinding with a positive u-velocity, $F = 0$ gives central differencing and $F = -1$ gives complete upwinding with a negative u-velocity. The space step sizes are dy and dx, the density is ρ and the pressure in the cell i, j is $p_{i,j}$. The y-momentum transport is calculated in the same way. The value chosen for the upwinding factor F has been selected after numerical experiment. The value is taken as a function of the local Mach number M:

$$F = 0{\cdot}5[1{\cdot}0 - \exp(-1{\cdot}36743M)] + \exp(-3{\cdot}7671M^2). \tag{2}$$

As well as transporting momentum between adjacent cells, the pressure gradients are also doing work if the local velocity is non-zero and hence transporting energy between the cells. This energy transport is obtained from the momentum transport calculated in (1) by multiplying by the local velocity.

The third phase of the mass, momentum and energy transport algorithm is the convection of the cells. This is illustrated in Figure 1 for convection with positive velocities u and v. A cell is regarded as moving with unchanged dimensions relative to the mesh of cell boundaries, so that it overlaps adjacent cells. The letter A indicates the area of a cell which remains in the original cell at the end of the time step, while B, C and D represent the areas of a cell which are located in adjacent cells. The quantities of mass, momentum and energy in the cell are divided in proportion to the areas A, B, C and D. Those proportions represented by B, C and D are subtracted from the quantities in the original cell and added to the appropriate adjacent cells.

When the adjustment of mass, momentum and energy has been completed for all cells, the flow variables ρ, u, v, p and t can be calculated for all cells.

FLOW OVER BLUNT BODY OF REVOLUTION

A cylinder is placed with its axis parallel to the incident supersonic flow. A detached bow shock and a downstream oblique shock, which is approximately conical far downstream, develop. The simulation was carried out in a domain of 499 cells by 199 cells with a body of revolution 25 cells in radius and so at lower Mach numbers the downstream oblique part of the shock is outside the simulated region. Results are presented for Mach numbers of 1·177, 1·69 and 6·0. The gas is a perfect viscous gas with ratio of specific heats $\gamma = 1{\cdot}4$ and Prandtl number 0·72: the gas is intended to represent air. The same gas properties, including viscosity, were used for all simulations reported, so the Reynolds number varies with the freestream velocity. The Reynolds number based on freestream conditions and body diameter is 7000 at Mach 1·177, 10,000 at Mach 1·69 and 35,500 at Mach 6·0. The algorithm has previously been used at higher Reynolds numbers:[4] increasing the Reynolds number results in the algorithm using shorter time steps and so a low Reynolds number was selected for these simulations.

For each Mach number contours of density and temperature are given (Figures 2–12) together with a graph of the temperature profile along the stagnation streamline. The wall temperature on the body is held at 1·0, the inlet temperature, and so there is a sharp temperature boundary layer along the wall. This is clearly visible in both the temperature contour plots and the temperature profiles.

Measured shock positions, taken from experimental data quoted by Liepmann and Roshko,[5] are shown on the temperature profiles (Figures 4, 8 and 11). At Mach 1·177 the shock has a thickness of about 30 cells. The shock thickness is less at high Mach numbers, reducing to about 10 cells at Mach 6·0. The temperature profile rises smoothly from the shock to the stagnation point in all flows.

The contour plots shown for Mach 6·0 (Figures 10–12) are taken at a time when the flow has not fully developed. The initial mismatched travelling normal shock system can be clearly seen at the downstream, right-hand side of the Mach 6·0 contour plots. However, the shock has developed around the stagnation point and has very close to the correct shock stand-off.

Plots with a limited number of Mach number contours are given for each Mach number to indicate the location of the sonic line relative to the shock (Figures 5, 9, and 12). At Mach 1·177 the sonic line is calculated to be approximately parallel to the front face of the bluff body and exits the calculation region across the upper boundary. The accuracy of the simulation will be

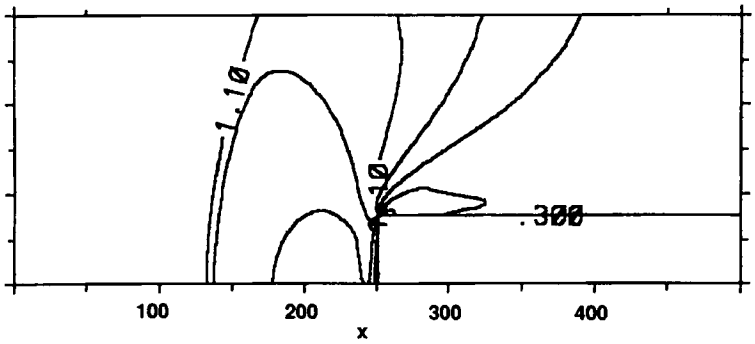

Figure 2. Density ratio contours for axisymmetric blunt body at Mach 1·177. Contours from 0·1 at intervals of 0·2.

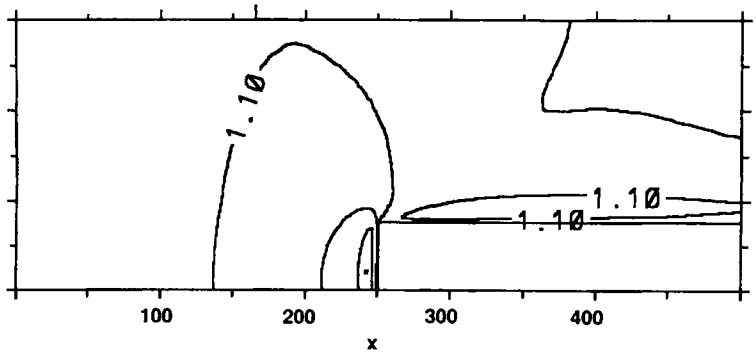

Figure 3. Temperature ratio contours for axisymmetric blunt body at Mach 1·177. Contours from 0·1 at intervals of 0·2.

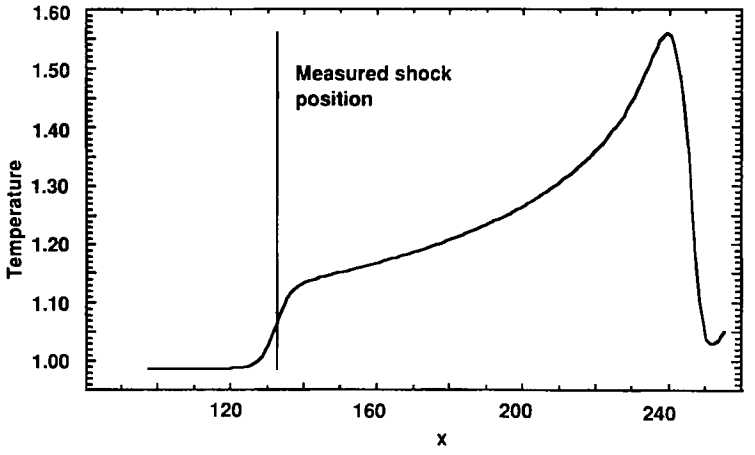

Figure 4. Temperature profile along centreline for axisymmetric blunt body at Mach 1·177. Measured shock position is taken from Reference 5.

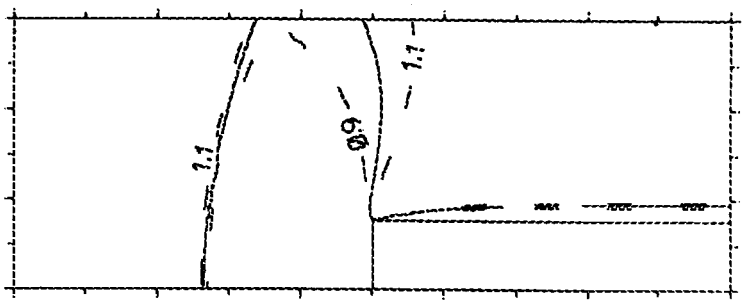

Figure 5. Mach number contours showing sonic line for axisymmetric blunt body at Mach 1·177. Solid contour, $M = 1{\cdot}0$; dashed contours, $M = 0{\cdot}9$ and $1{\cdot}1$.

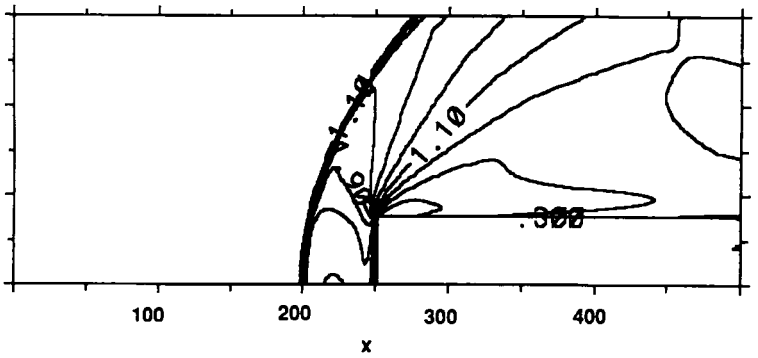

Figure 6. Density ratio contours for axisymmetric blunt body at Mach 1·69. Contours from 0·1 at intervals of 0·2.

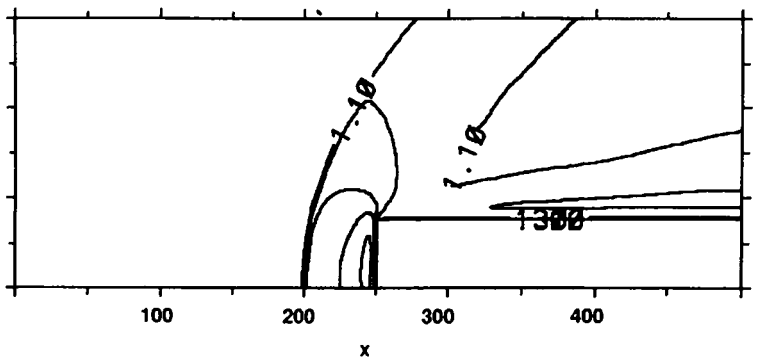

Figure 7. Temperature ratio contours for axisymmetric blunt body at Mach 1·69. Contours from 0·1 at intervals of 0·2.

reduced by this, since the free boundary condition applied is only valid for supersonic flow. However, experience with other transonic flows indicates that the free boundary condition is satisfactory with small regions of subsonic flow on the free boundary. At higher Mach numbers the sonic line is much reduced in extent and joins the detached shock, nearer the body and well within the computation region. While no comparisons with measurements are made, the general behaviour and location of the sonic line are in accord with observations.[5]

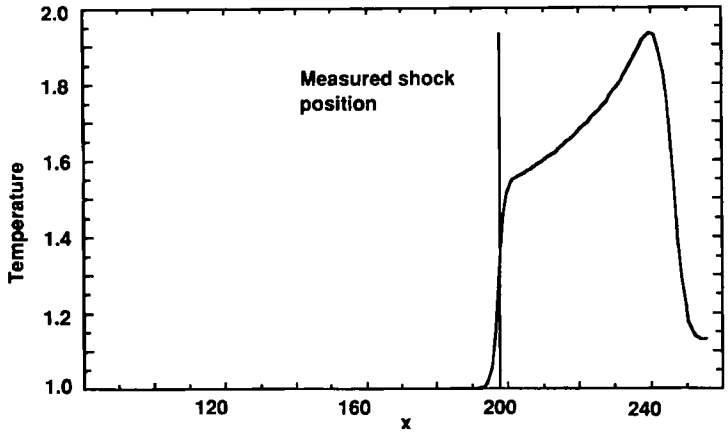

Figure 8. Temperature profiles along centreline for axisymmetric blunt body at Mach 1·69. Measured shock position is taken from Reference 5.

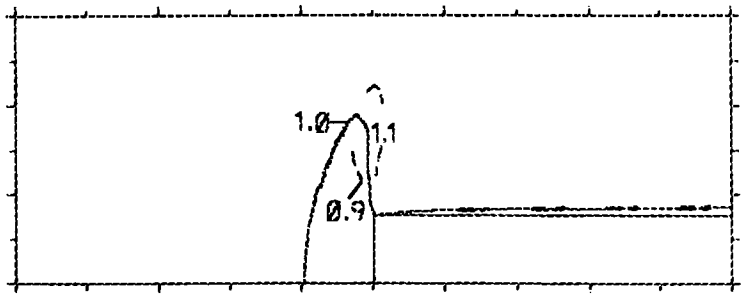

Figure 9. Mach number contours showing sonic line for axisymmetric blunt body at Mach 1·69. Solid contour, $M = 1{\cdot}0$; dashed contours, $M = 0{\cdot}9$ and $1{\cdot}1$

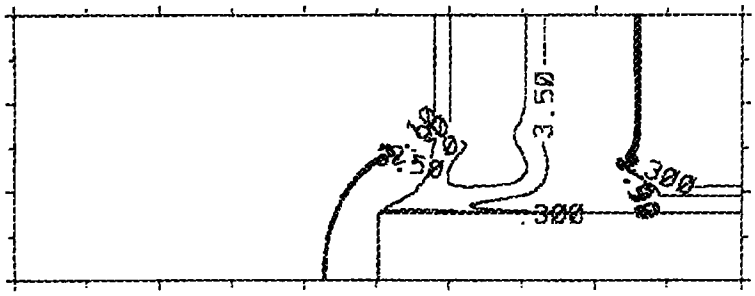

Figure 10. Temperature ratio contours for axisymmetric blunt body at Mach 6·0. The flow has not reached steady state, but the detached shock is at the fully developed stand-off distance. Contours from 0·1 at intervals of 0·2

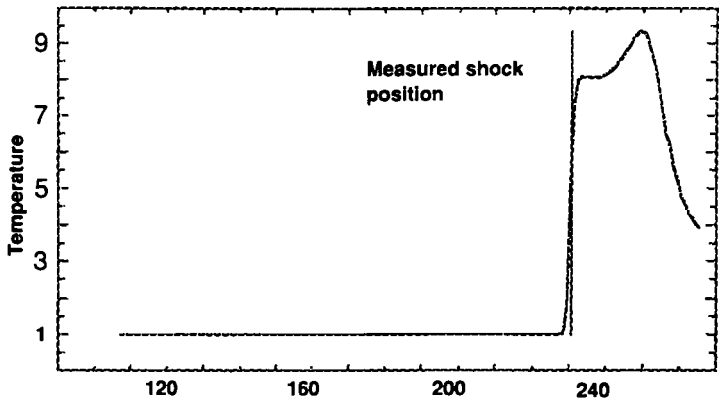

Figure 11. Temperature profile along centreline for axisymmetric blunt body at Mach 6·0. Measured shock position is taken from Reference 5

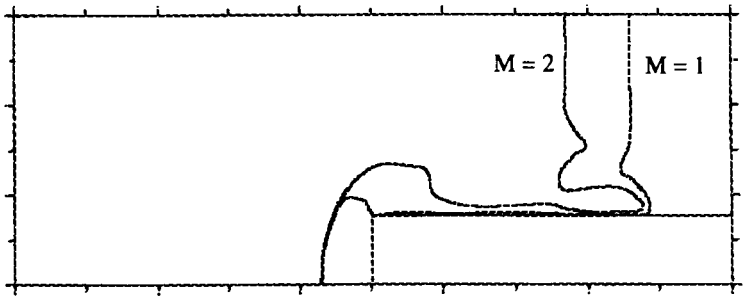

Figure 12. Mach number contours showing sonic line for axisymmetric blunt body at Mach 6·0. The flow has not reached steady state, but the detached shock is at the fully developed stand-off distance. Contours $M = 1{\cdot}0$ and 2·0

FLOW OVER SPHERE

Predictions are reported for a sphere in axisymmetric flows with Mach numbers of 1·177 and 1·69. As with the axisymmetric blunt body, the sphere has a wall temperature held at 1·0, equal to the inlet temperature. The calculations were performed in a region of 499 cells by 199 cells and the sphere has a radius of 25 cells. The gas is a perfect viscous gas with ratio of specific heats $\gamma = 1{\cdot}4$. The flows shown for Mach numbers of 1·177 and 1·69 are fully developed. Contours of density and Mach number as well as temperature profiles along the stagnation streamline are shown (Figures 13–18). The sonic line can be distinguished in Figure 14 for Mach 1·177 and in Figure 17 for Mach 1·69. At Mach 1·177 the sonic line exists the computation region over the free upper boundary and the calculation will have an incorrect boundary condition where the exiting flow is subsonic. Nevertheless, the predicted stand-off distance compares well with experiment.[5]

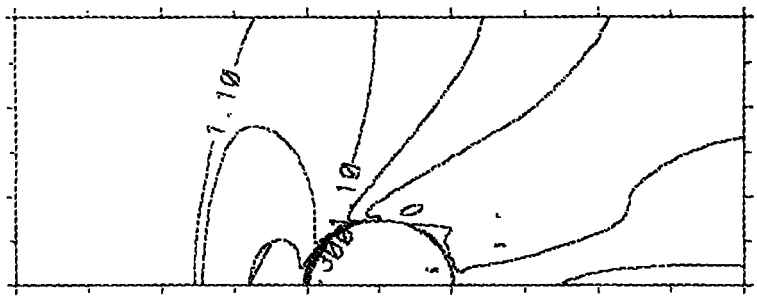

Figure 13. Density ratio contours for sphere at Mach 1·177. Contours from 0·1 at intervals of 0·2

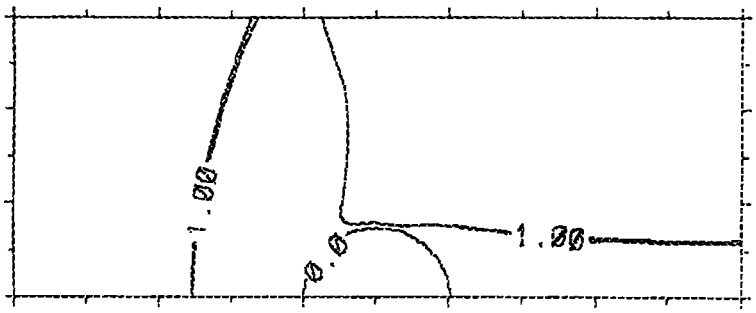

Figure 14. Mach number contours showing sonic line for sphere at Mach 1·177. Contours M = 1·0 and 1·05

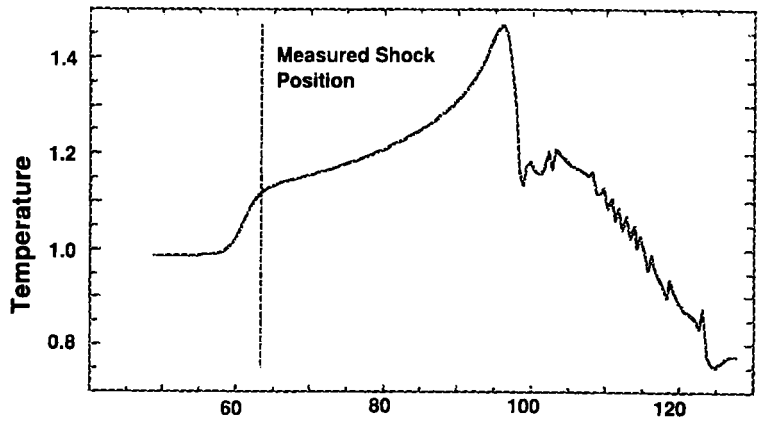

Figure 15. Temperature profile along centreline for sphere at Mach 1·177. Measured shock position is taken from Reference 5

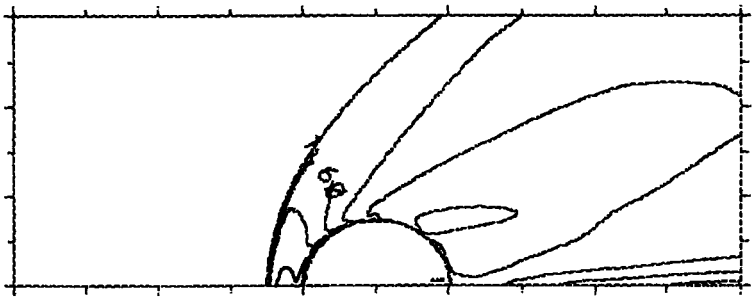

Figure 16. Density ratio contours for sphere at Mach 1·69. Contours from 0·0 at intervals of 0·4

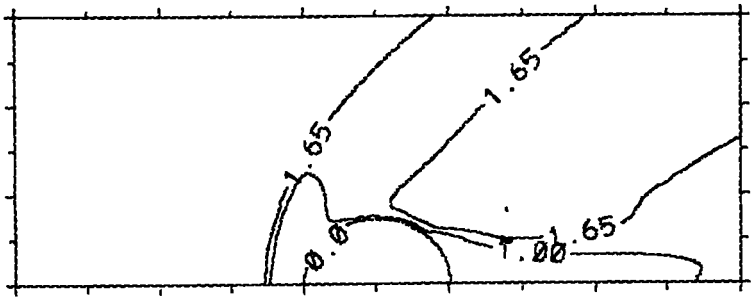

Figure 17. Mach number contours showing sonic line for sphere at Mach 1·69. Contours $M = 1{\cdot}0$ and 1·65

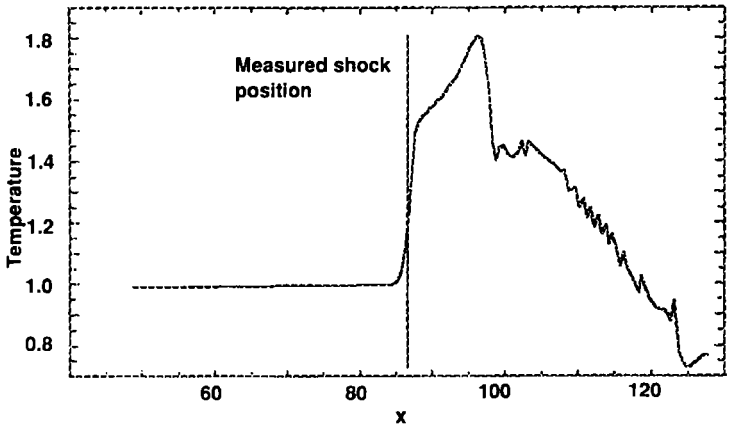

Figure 18. Temperature profile along centreline for sphere at Mach 1·69. Measured shock position is taken from Reference 5

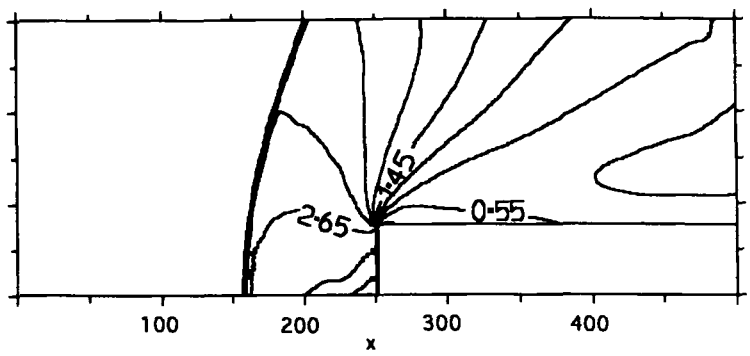

Figure 19. Density ratio contours for blunt-edged flat plate at Mach 1·69. Contours from 0·05 at intervals of 0·3

FLOW OVER BLUNT PLATE

The examples previously given are for axisymmetric flows. As an example of two-dimensional flow, a simulation of the flow past a blunt-edged plate at Mach 1·69 is given. Density contours are shown in Figure 19. The gas is a perfect viscous gas with ratio of specific heats $\gamma = 1{\cdot}4$ and the wall temperature is held at the inlet temperature. The flow is not quite fully developed and has only developed about 76% of the experimental stand-off distance. The convex shape of the density contours around the stagnation point is characteristic of this early stage of the flow development. The expansion at the corner of the plate is clearly formed.

COMPARISON WITH EXPERIMENTAL DATA

A large series of shock stand-off measurements are reported by Liepmann and Roshko[5] and these data are reproduced in Figure 20. The simulations performed for this paper are reported

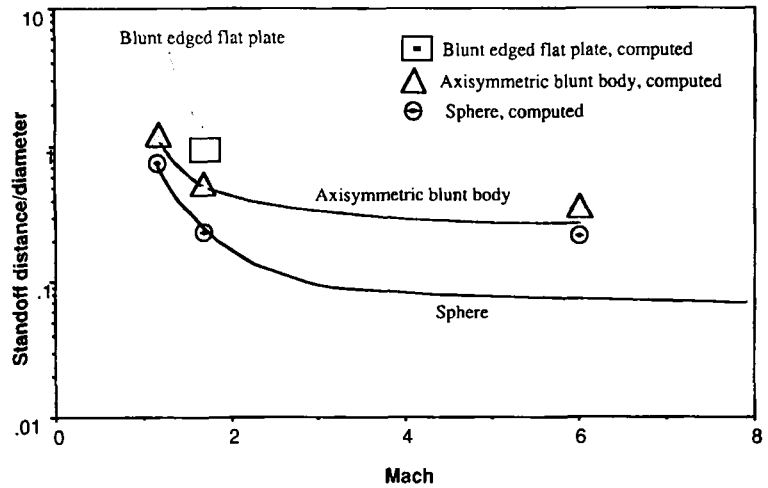

Figure 20. Comparison of computed and measured steady state shock stand-off distances for a variety of bluff bodies in supersonic flow of a perfect gas

in the same figure. A result for a sphere at Mach 6·0 is shown, but this is at a very early stage of the calculation. It is interesting that at this Mach number the early results overpredict the stand-off distance: it is regretted that the calculation has not yet been performed to steady state, since other demands on the computer used have prevented continuation of the calculation. It can be seen that reasonable agreement is obtained in most cases and that where the flow has fully developed the agreement is extremely good.

CONCLUSIONS

The algorithm described has been shown to give satisfactory simulations of viscous, perfect gas flows with detached shocks at Mach numbers ranging from low supersonic to hypersonic values. Considerable testing is required to confirm the accuracy of the algorithm for flows with detached shocks in other geometries. The algorithm has the potential to be developed to incorporate real gas effects created by dissociation of and chemical reaction among molecules in high enthalpy flows and further work will proceed in this direction.

REFERENCES

1. J. F. Milthorpe, 'Simulation of supersonic and hypersonic flows', *Int. j. numer. methods fluids*, **14**, 267–288 (1992).
2. J. F. Milthorpe, 'Numerical simulation of two-dimensional compressible flows', in C. Taylor, J. H. Chin and G. M. Homsy, (eds), *Proc. 7th Int. Conf. on Numerical Methods in Laminar and Turbulent Flows*, Pineridge, Swansea, (1991).
3. J. F. Milthorpe, 'Numerical simulation of two-dimensional and axisymmetric compressible flows', in K. Takayama (ed), *Proc. 18th Int. Symp. on Shock Waves*, Springer, Berlin, (1992).
4. J. F. Milthorpe, 'Numerical simulation of two-dimensional compressible flows', *Int. J. Numer. Methods Heat Fluid Flow*, **3**, 223–231 (1993).
5. H. W. Liepmann and A. Roshko, *Elements of Gasdynamics*, Wiley, New York, (1957).